Stress corrosion cracking resistance of type 316L(N) stainless steel weld joints

M. Ragavendran[*1,2], Anita Toppo[3], and M. Vasudevan[1,2]
[1]Homi Bhabha National Institute,
[2]Metallurgy and Materials Group,
[3]Atal Incubation Centre, Safety, Quality and Resource Management Group

Indira Gandhi Centre for Atomic Research, Tamil Nadu, India
*mragavendran@igcar.gov.in, *anita@igcar.gov.in, dev@igcar.gov.in*

Abstract: Stress corrosion cracking resistance (SCC) of AISI type 316L(N) stainless steel weld joints fabricated using conventional TIG and Activated-TIG (A-TIG) welding processes are evaluated and compared with the 316L(N) base metal. Delta ferrite (ä ferrite) measurements and tensile tests were carried out for TIG and ATIG weld joints. SCC tests were carried out using a constant load testing technique at 60% yield strength (YS) of the material. Testing environment was concentrated solution of sodium chloride acidified using hydrochloric acid. SCC results indicated superior resistance of 316L (N) base metal compared to TIG and ATIG welds. Inferior corrosion resistance of welds is attributed to the presence of δ ferrite in the welds. ferrite results in increased microstructural and microchemical heterogeneities in weld metal as compared to a base metal. Among the weld joints, A-TIG exhibited higher resistance to SCC than the TIG due to the (austenitic-ferritic) AF solidification mode, and to the resultant microstructure produced autogenously in a single pass. On the other hand, the presence of a higher amount of δ ferrite and multipass welding of TIG welds causes extensive segregation of sulphur and phosphorous at the ferrite/γ austenite interfaces. Interfaces acts as pre-existing active paths along which corrosive attack progresses. It causes degradation in localised corrosion resistance of conventional TIG. Time to failure is high for base material (446 hrs) followed by A-TIG weld joint (306 hrs) than the TIG weld joint (232 hrs). Therefore A-TIG welding is preferable to fabricate the structural components and sodium carrying pipes in the nuclear industry than the conventional TIG welding process.

Keywords: A-TIG Welding, 316(L) N Stainless Steels, Stress Corrosion Cracking.

1 Introduction

The nuclear grade structural materials require a combination of high-temperature strength, irradiation stability and strong corrosion resistance. AISI 316L(N) has own these properties and extensively used to produce nuclear reactor components. Welding is used for the fabrication of the massive structures. There are different welding processes, each has specific advantages and disadvantages. Currently, the arc welding process is used, but it has several demerits such as higher residual stress and distortion induced due to higher heat input [1]. The arc emanating from the heat source spreads widely and produces more damages to the nearby base metal.

The novel variant of the TIG (Tungsten Inert Gas) welding process called A-TIG (Activated-Tungsten Inert Gas) uses activated flux to enhance weld depth penetration [2]. Mostly oxide-based activated fluxes are used, and it is blended with a binder to form a paste. This paste is applied over the plates to be welded. Maximum of 12 mm thick plates can be welded in a single pass autogenously in square butt configuration. Penetration enhancement is due to the reversal of Marangoni convection, and Arc constriction by applying activated flux. Due to arc constriction, the heat dissipation losses are low, melting efficiency is high, and all heat input is utilized to produce the weld [3]. Since the weld joint is made in a single pass with small weld metal volume, the distortion and other weld deformations are low. A-

TIG welding's main advantages are no edge preparation, high welding speed, and no filler wire consumption. All these lead to increased productivity and high-quality welds economically.

The massive nuclear structure contains welds in more number, which are more prone to stress corrosion cracking (SCC) [4]. It occurs because of the synergistic active interaction among the stress, material and the environment. Generally, AISI 316L(N) steel has high resistance towards uniform or general corrosion. However, they are less immune to SCC than the ferritic stainless steels because of its high coefficient of thermal expansion and low thermal conductivity [5]. It induces more stress and distortion due to welding. Base materials electrochemical properties are entirely different from the welds, the weakest link in the structure. Welds are more heterogeneous in all aspects than the base material. The main factors which influence SCC behaviour are the materials composition, weld chemistry, stress content, microstructure, distribution and morphology of the second phases present in the weld [6]. Welding process has a significant influence on the weld metal SCC. Each welding process differs from one another in producing the welds. Heat input and associated cooling rate vary from one welding to another technique. AISI 316L(N) welds produced by different welding process exhibits variations in solidification mode, weld metal and secondary phase volume.

The main secondary phase in 316L(N) weld is δ ferrite. It has different morphology and distribution, which depends on the type of welding process employed. The existence of δ ferrite in austenite welds should be in optimum level and when it is distributed uniformly in the weld it is beneficial in improving the resistance towards SCC [7, 8]. The literature available is limited in the area of SCC behaviour and time to failure assessments for weld joints produced by advanced welding process such as A-TIG. In the present work, AISI 316L(N) weld joints are fabricated by two different welding techniques: TIG and A-TIG welding processes. SCC resistance evaluation of these joints is carried out systematically and the results are compared with the base metal.

2 Experimental

The material used in this research work is type AISI 316L(N) austenitic stainless steel having a dimension of 300 mm x 125 mm x 5.6 mm. V- groove is prepared for conventional multi-pass TIG welding to accommodate type 316L filler wire, whereas square edge butt configuration without groove preparation is utilized for A-TIG welding. Plate dimensions and groove configuration details are given in **Fig. 1**. Thermocouples are fixed in the plates to determine the cooling rate. Base material and fabricated welds chemical composition is shown in **Table 1**. The welding process parameters employed for fabricating joints are provided in **Table 2.**

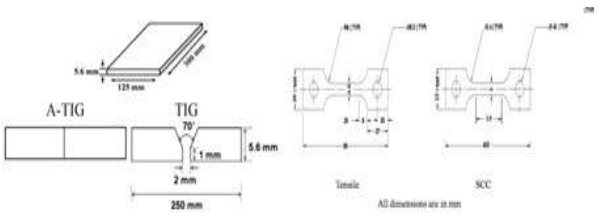


Fig. 1. Groove preparation, flat tensile and SCC specimen dimensions

Table 2. Welding parameters

Welding process	Passes	Current, A	Voltage, V	Torch speedmm/ sec	Heat input, kJ/mm
TIG	4	93	11	0.9	0.7
A-TIG	1	180	13	1.6	0.9

Table 1. Chemical composition of 316L (N) base metal and different weld joints

Sample	C	N	S	P	Mn	Ni	Cr	Mo	Nb	Si	Co	V	Ti	Cu	Fe
Base Metal	0.02	0.09	0.01	0.02	1.6	12.4	17.2	2.3	0.07	0.44	0.14	0.13	0.08	0.15	Balance
TIG	0.03	-	0.01	0.02	1.53	12.3	18.27	2.31	0.04	0.38	0.10	0.10	0.002	0.15	Balance
A-TIG	0.02	0.08	0.001	0.02	1.67	12.21	16.88	2.32	0.04	0.48	0.10	0.10	0.002	0.3	Balance

A-TIG welding process was made without filler wire addition, in a single pass whereas; TIG process uses wire addition (316l) in a multi-pass welding. The welds had passed radiographic examination and bend tests. Blanks for making specimens for tensile and stress corrosion tests were cut from these weld pads to contain weld joint. Flat tensile specimens as shown in Fig. 1 were fabricated to carry out tensile and stress corrosion cracking test. Weld joints were electrochemically etched in equal amounts of nitric acid and demineralised water at 2V for 10 seconds. The as-welded specimens were then examined in an optical and scanning microscope for its microstructure. The tensile test at $3 \times 10^{-4}s^{-1}$ strain rate is carried out to find out the yield strength of joints. The δ ferrite content in the welds is measured using fisher make ferritescope, which works on the principle of magnetic induction. Once the weld joints are fabricated, it is cleaned with acetone to remove the dirt and contaminants. About 40 measurements are taken along the weld, and the average ä ferrite content in ferrite number (FN) is reported. SCC studies were carried out for 316N SS base metal and for 316L(N) welds prepared using different techniques in boiling 5 M NaCl + 0.15 M Na_2SO_4 solution acidified with 2 ml/l of concentrated HCl (boiling point = 381.5 K; pH = 1.3). Constant load testing technique was used to carry out SCC studies and time to failure (t_f) was used as the assessment criterion. During SCC, linear variable differential transformer (LVDT) was fixed to the wave guide welded to the specimen undergoing SCC, which logged the elongation with respect to time data. SCC studies were carried out at 60% of the Yield strength(YS) of material. This solution simulates the actual environment, and the addition of HCl aggravates the cracking and Na_2SO_4 helps repassivation. The fractured surfaces were examined using a scanning electron microscope (SEM) to study the SCC failure mode.

3 Results and Discussion

Chemical composition of welds was analyzed using energy dispersive spectroscopy and is shown in Table 1. Nitrogen loss was observed in TIG welding processes whereas, ATIG, weld joint are produced without nitrogen loss compared to the base metal. This may be due the presence of strong ferrite stabilizers in the TIG weld. Since, nitrogen is a strong austenite stabilizer; presence of these ferrite stabilizers will suppress the austenite stabilizers in the welds. Details are discussed elaborately in solidification mode section. Chromium content and nickel content also varied slightly for these different weld joints which may influence the localized corrosion properties of 316L(N) SS weld joints.

3.1 Microstructure

TIG and A-TIG welds macrostructure and microstructure is shown in **Fig. 2 (a-d). Fig. 2a and b** shows the macrostructures of the transverse section of A-TIG and TIG weldments. A-TIG (**Fig. 2b**) macrostructure shows single-pass deposition, whereas TIG weld **Fig. 2a** shows four passes deposition. Both kinds of welds are free from macroscopic defects and also show good penetration. Higher weld metal volume containing more amount of ä ferrite, and heterogeneous microstructure because of filler wire addition in multiple passes, makes TIG weld joint more susceptible to localised corrosion attack than the A-TIG weld joint. On the contrary, A-TIG joint fabricated in a single pass has lower weld metal volume, the symmetrical weld geometry and homogenous microstructure. A-TIG weld centre contains very fine equiaxed shaped grains which grow in the welding direction is sandwiched between the columnar grains.

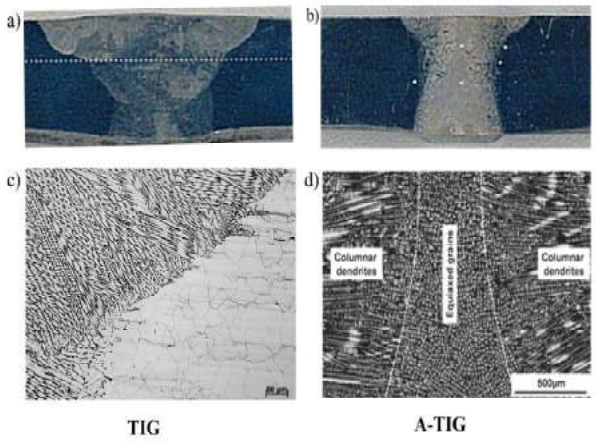


Fig. 2. Weld macrograph compared with FEM model

Fig. 2. TIG and A-TIG welds macro and microstructure

3.2 Solidification Mode and Ferrite Number

The type of welding process employed, whether autogenous or with filler wire, including process

Table 3. Calculated Cr_{eq}/Ni_{eq} for welds using different formulas

Name	$\frac{Cr_{eq}}{Ni_{eq}}$	TIGweld	A-TIG weld
Schaeffler	$\frac{Cr + Mo + 1.5Si + 0.5Nb}{Ni + 0.5Mn + 30C}$	1.50	1.43
Delong's	$\frac{Cr + Mo + 1.5Si + 0.5Nb}{Ni + 0.5Mn + 30(C + N)}$	1.50	1.21
Hammar & Svensson's	$\frac{Cr + 1.37Mo + 1.5Si + 2Nb + 3Ti}{Ni + 0.31Mn + 22C + 14.2N + Cu}$	1.61	1.39
WRC 1992	$\frac{Cr + Mo + 0.7Nb}{Ni + 35C + 20N + 0.25Cu}$	1.52	1.27

parameters, significantly decides the solidification mode. Cr equivalent (Cr_{eq}) and the Ni equivalent (Ni_{eq}) which are derived from the formula such as Schaeffler [9], Delong [10], Hammar & Svensson's [11], WRC 1992 [12] can show the complexities of solidification. The ratio of the Cr_{eq} and the Ni_{eq} of the stainless steel were calculated using the formula's given in **Table 3**. The Cr_{eq} is assessed using ferrite stabilizer and Ni_{eq} by austenite stabilizers. The ratio of the Cr_{eq} and the Ni_{eq} of the stainless steel is shown in **Table 3.** Usually as the Cr_{eq}/Ni_{eq} ratio increases, the ferrite forming tendency of the stainless steel increases. Based on these observations, TIG welding process which was carried out in multiple passes using filler wire and which contains more amounts of ferrite stabilizers than the base material. TIG weld exhibited FA mode (primary ferritic) which resulted in continuous ferrite network precisely representing the cleavage plane having high-stress concentration, resulted in the FA solidification mode. On the other hand, A-TIG joint is produced autogenously in a single pass. A-TIG weld manifested AF mode (primary austenitic) producing finer δ ferrite in meagre amounts which is validated by the ferrite measurements. Different solidification mode produces ferrite with distinct morphologies which depends on the welding process and chemical composition.

Ferritescope measurements are in line with the calculated Cr_{eq}/Ni_{eq} ratio, where TIG weld showed highest δ ferrite content than the A-TIG weld. There was no ferrite content observed in base metal. δ ferrite is influenced by filler metal [13] and welding process parameters such as higher cooling rates and lower heat input. Since, TIG welds were prepared using filler wire which contains higher amount of ferrite stabilizers; hence, it shows increased ferrite content. Whereas, ATIG weld showed minimal ferrite content. The cooling rate and ferrite content in both the welds are shown in **Table 4**. Cooling rate mainly affects the phase formation - solidification mode and morphology, which determines the final mechanical behavior of the weldments.

Table 4. Calculated cooling rate and ferrite number for welds

Weld	Cooling Rate, °C/s	FN
TIG	4.06	5
A-TIG	12.52	1

Compared with A-TIG, in TIG welding, a low amount of heat input is delivered in a single pass. Still, heat input utilized to form a joint is high for TIG welding because of multiple recurring passes. It results in lower cooling rates in TIG welding, whereas the weld joint produced in a single pass by A-TIG welding has low heat input resulting in a higher cooling rate. This higher cooling rate suppressed the secondary phase such as δ ferrite formation by not allowing sufficient diffusion time and made the weld solidify by AF solidification mode. On the contrary, the lower cooling rate in TIG welds gives adequate time for δ

ferrite formation, and the high amount of ferrite stabilizers caused the weld to solidify in FA mode.

3.3 Tensile properties

Type of welding process employed and weld metal composition significantly influences the tensile properties of the weld joints. Since welding produces gradients in chemical composition, it drastically controls the phases, and microstructural constituents formed in the weld depend on the solidification mode that decides the mechanical behaviour of joints. The tensile results are shown in **Fig. 3.** Base materials tensile results are significantly better than the weld joints. Base material exhibited the highest UTS than the joints, and it is attributed to their work-hardening behaviour. TIG weld displayed higher UTS than the A-TIG joint due to the higher amount of δ ferrite, which impedes the dislocation motion, thereby increasing the UTS. Base material exhibited the lowest yield strength than the weld joints, because of the uniform microstructural homogeneity and devoid of δ ferrite. Presence of δ ferrite influences the mechanical properties of the weld joints. TIG weld joint exhibited the highest yield strength. It is attributed to the higher amount of δ ferrite in the TIG weld, which is confirmed by the ferrite measurements. A-TIG weld joint showed lowest yield strength as a result of presence of meagre amounts of ä ferrite. Grain size and dendrite arm spacing also influences the tensile strength of the material. Like grains in the base material, weld contains dendrites which are characterized by their arm. The dendrite arm spacing in welds depends on the cooling rate and associated chemical composition. Low heat input per pass in TIG welding results in low dendrite arm spacing of 5.72 µm, resulting in higher yield strength in TIG weld joint. In comparison, high heat input in a single pass in A-TIG weld causes the coarsening of dendrite arms and forms high arm spacing of 7.97 µm and the microstructures of welds showing dendritic features are shown in **Fig. 4.**

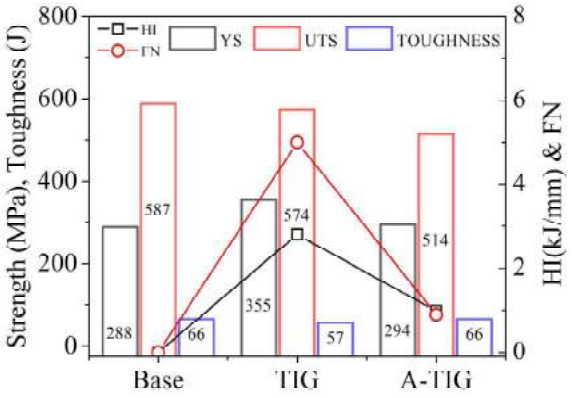


Fig. 3. Tensile and toughness results

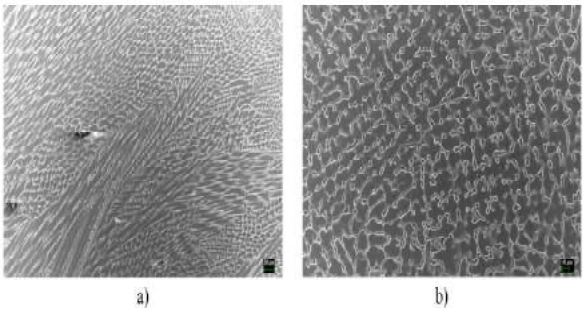


Fig. 4. Dendrite arm spacing in welds a) TIG b) A-TIG

3.4 SCC

SCC resistance of 316LN base metal was higher than the welds prepared using different welding process and is shown in Fig. 4b. This could be due to microstructural and microchemical heterogeneities in the weld metal as compared to the base metal. Mill annealed 316LN base metal have an even distribution of the alloying elements in the austenite matrix. The presence of δ ferrite in the weld metal causes partitioning of major alloying elements - ferritisers, such as Cr and Mo getting concentrated in ä ferrite while austenitisers, like Ni, C, N, partitioning into the austenite [14, 15]. Besides partitioning of alloying elements, segregation of S and P occurs at the δ ferrite/ γ austenite interface [16]. Also, the weld metal is a cast structure with a high concentration of microscopic defects such as dislocations and vacancies. Also, welding defects, such as inclusions, are present in the weld metal. All these result in formation of an uneven and weakly adherent passive film on the surface of the weld metal

Table 5. SCC time to failure and corrosion elongation curve parameters for 316L(N) base metal, TIG and A-TIG weldments

Material	Applied tensile stress 0.6*(YS),MP a	Yield stress, MP a	Time to failure t_f,hrs	Time to transition $t_{ss,}$ hrs	t_{ss}/t_f	Crack growth rate,mm²/hr
Base material	173	288	446	244	0.547	0.0175
TIG	213	355	232	112	0.482	0.0225
ATIG	176	294	306	140	0.457	0.0138

as compared to the base metal. On comparing the SCC resistance of welds of ATIG and TIG weldment of 316L(N) SS, A-TIG weldment showed superior resistance. Welding causes gradients in composition and microstructural features in the weld, which drastically affects the SCC performance based on the phases produced through the solidification mode. The microstructure of the weldments significantly affects localised corrosion behaviour. The microstructural features influence the passive layer formation, its stability and electrochemical behaviour that substantially decides the susceptibly to SCC. Moreover, it affects the formation and developments of the pit from which the cracks can initiate, propagate, and eventually produce severe SCC. These microstructural features are the highest obstacles for SCC crack initiation and propagation. SCC behavior of a weldment is influenced by a variety of factors, which include amount, size, morphology and continuity of the δ ferrite network, residual stresses and metallurgical defects present in the weld metal, alloy element partitioning and segregation at the γ /δ ferrite interfaces. Finer δ ferrite distribution in A-TIG welds gives a high resistance to SCC, and γ austenite - δ ferrite interface acts as crack arrestor. A continuous network of δ ferrite in TIG welds is harmful and promotes SCC.

The stress corrosion cracking and corrosion elongation details are shown in **Table 5**. When a constant load was applied to a specimen at a constant temperature, a continuous increase in elongation was observed, finally leading to fracture as shown in **Fig. 5**. This elongation vs. time curve is referred to as corrosion creep curves by researchers [17]. These corrosion elongation curves can be divided into three regions i.e. primary, secondary and tertiary regions. In the primary and tertiary region there is increase in the elongation with increasing time. The elongation rate in the secondary region remains constant and is referred as steady state elongation rate. **Fig. 5** shows the schematic corrosion elongation curve and the curves for base material and the weld joints.

From **Fig. 6** it is observed that time to failure is high for base material than the weld joints. A-TIG joint manifested higher time to failure than the TIG joint. It is due to δ ferrite's presence, and it significantly influences the SCC behavior of the weld joints. δ ferrite volume, distribution, including morphology, plays a crucial role in deciding the weld's resistance to SCC. Time to transition from secondary to tertiary is also higher for base material followed by A-TIG than TIG joint. Homogenous microstructure containing finer amounts of δ ferrite in A-TIG weld having low weld metal volume is responsible for producing higher time to failure than the TIG joint.

Fig. 7 shows the t_{ss}/t_f ratio for the base material and the weld joints, which clearly indicates that this ratio is higher for base material than the weld joints. In base material, t_{ss} is high, which results in higher t_{ss}/t_f ratio. For A-TIG joint, t_f is high, which yielded low ratio.

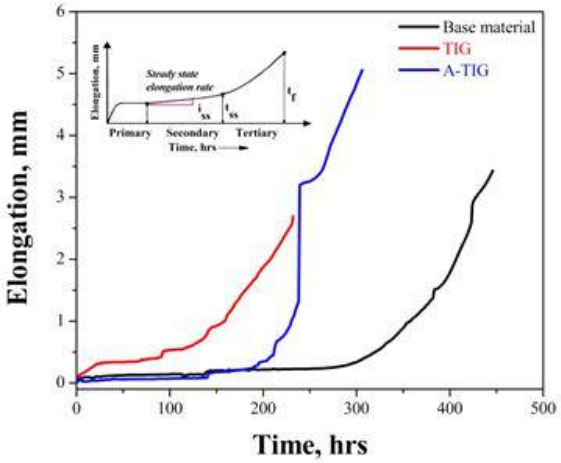


Fig. 5. Corrosion elongation curve for base material and weld joints

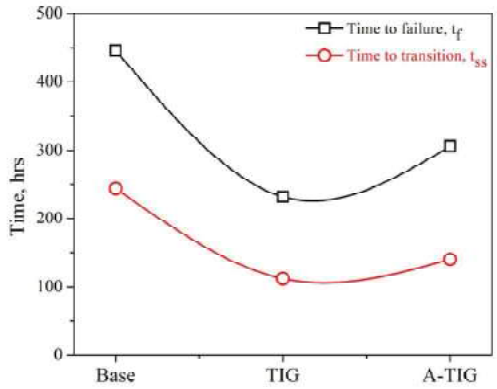


Fig. 6. Time to transition and time to failure for base material and weld joints

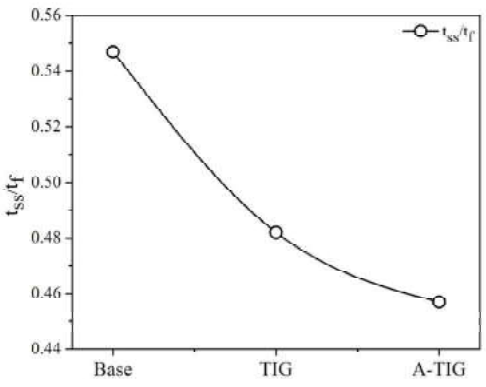


Fig. 7. Corrosion elongation curve for base material and weld joints

The corrosion creep crack growth rate (CGR) can be calculated using the below-mentioned formula [18]

$$Vc = \frac{cracking\ surface}{propagation\ time} = \frac{S_0}{t_p}\left(1 - \frac{\sigma}{\sigma_r}\right)$$

where S_0 = sample initial cross-section, t_p = propagation time, σ = initial stress and σ_r = ultimate tensile strength.

Apart from microstructure, yield strength of the materials also influence, SCC resistance of the materials. The YS of material increases, its plastic zone size decreases which will result in formation of sharp crack ahead of the crack tip. Contrary to this when the YS is lower, the plastic zone size would be higher resulting in better stress relaxation causing increased SCC resistance [8]. Since TIG weldment has higher YS, cracks formed ahead of the plastic zone will be sharper and hence, faster crack initiation will take place. Whereas, A-TIG weldment with lower YS values and with lager plastic zone size, more time is required for sharpening of the crack and hence, delayed crack initiation. **Fig. 8** shows the one-to-one correspondence between the YS and CGR in the base material and weld joints. Higher the yield strength, higher will be the crack growth rate.

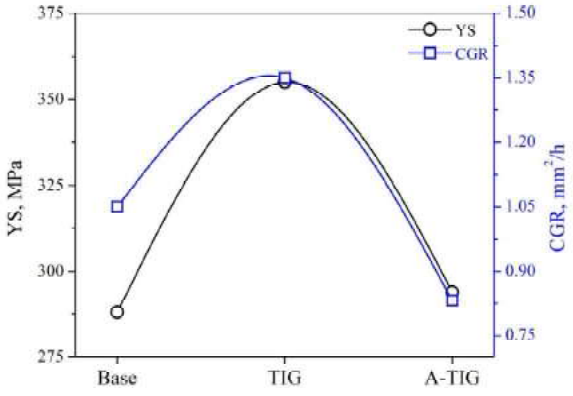


Fig. 8. Corrosion elongation curve for base material and weld joints

The fractographs of the base material and weld joints are shown in **Fig. 9**. It is observed that base metal as well as weldments failed by transgranular mode of SCC failure. The transgranular cracking observed

in the weldments is typical of the one observed in chloride environments [19–21]. These fan-shaped patterns may be the result of "microbranching" of a stress corrosion crack in certain crystallographic planes when it comes across a region of misorientation such as grain boundaries or twin boundaries. The crack will then propagate in a number of parallel planes showing crack branching in the microstructure [20, 21].

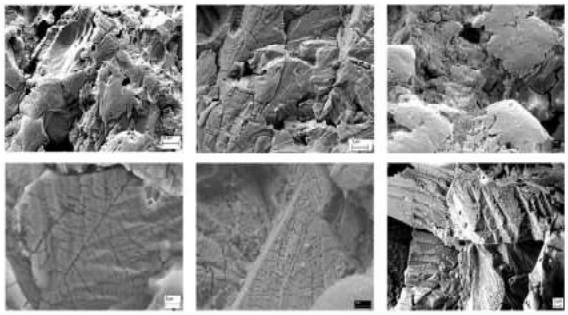


Fig. 9. SCC fractographs

4 Conclusions

In this research work, the SCC test of Type 316L(N) austenitic stainless steel weld joints made of conventional TIG and A-TIG welding processes is studied. Boling acidified sodium chloride was used to evaluate the resistance to SCC behaviour. The results are compared with the base material. The conclusions are as follows.

- δ ferrite content and morphology strongly influence the mechanical properties such as tensile, toughness values and consequently the SCC behaviour.
- Higher the yield strength, higher will be the crack growth rate in SCC of the weld joints.
- Chemical composition and weld solidification mode drastically affect the SCC behaviour.
- AF mode has higher resistance than the FA mode it is attributed due to the formation of ferrite phase containing a high amount of chromium having high resistance to SCC.
- A-TIG weld joint exhibited a more prolonged time to failure than the TIG joint, owing to the low yield strength, low δ ferrite content and homogenous microstructure throughout the weld.
- A-TIG joint has sufficient strength, toughness on par with the base material and high resistance to SCC.

Therefore, A-TIG welding is recommended for fabricating the nuclear structural components when compared with the conventional TIG welding process.

References

1. Shenghai Z, Yifu S, Huijuan Q (2013) The technology and welding joint properties of hybrid laser-tig welding on thick plate. Opt Laser Technol 48:381–388. https://doi.org/10.1016/j.optlastec.2012.11.014
2. Vasudevan M, Bhaduri AK, Raj B, Rao KP (2007) Genetic-algorithm-based computational models for optimizing the process parameters of A-TIG welding to achieve target bead geometry in type 304 L(N) and 316 L(N) stainless steels. Mater Manuf Process 22:641–649. https://doi.org/10.1080/10426910701323342
3. Howse DS, Lucas W (2000) Investigation into arc constriction by active fluxes for tungsten inert gas welding. Sci Technol Weld Join 5:189–193. https://doi.org/10.1179/136217100101538191
4. Ding J, Zhang ZM, Wang JZ, et al (2015) Corrosion behavior of different parts of the weld of 316L/52M/A508 dissimilar metal welded joint in simulated pressurized water reactor primary water. Mater Corros 66:1435–1444. https://doi.org/10.1002/maco.201508448
5. Zhou N, Pettersson R, Lin Peng R, Schönning M (2016) Effect of surface grinding on chloride induced SCC of 304L. Mater Sci Eng A 658:50–59. https://doi.org/10.1016/j.msea.2016.01.078
6. Russell H. Jones, Ricker RE (1992) Mechanisms of Stress-corrosion Cracking. In: Stress-Corrosion Cracking Materials Performance and Evaluation. pp 1–40

7. Baeslack WA, Duquette DJ, Savage WF (1979) Effect of Ferrite Content on Stress Corrosion Cracking in Duplex Stainless Steel Weld Metals At Room Temperature. Corrosion 35:45–54

8. Shaikh H, George G, Schneider F, et al (2000) Stress corrosion crack growth studies on nitrogen added AISI type 316 stainless steel and its weld metal in boiling acidified sodium chloride solution using the fracture mechanics approach. Mater Corros - Werkstoffe und Korrosion 51:719–727. https://doi.org/10.1002/1521-4176(200010)51:10<719::AID-MACO719>3.0.CO;2-3

9. Schaeffler A.L (1949) Constitution diagram for stainless steel weld metal. Met Prog 56:680-680B

10. DeLong WT Ferrite in austenitic stainless steel weld metal. Weld J 53:273–286

11. Hammar O, Svensson U (1979) Solidification and Casting of Metals. In: Proceedings of an International Conference on Solidification. University of Sheffield, England, pp 401–410

12. KOTECKI D, SIEWERT T (1992) WRC-1992 constitution diagram for stainless steel weld metals/ : a modification of the WRC-1988 diagram. Weld J 71:171–178

13. Kou S (2003) Welding metallurgy. Hoboken: John Wiley & Sons

14. Lippold JC, Savage WF (1979) Solidification of Austenitic Stainless Steel Weldments/ : Part I — A Proposed Mechanism The distribution and morphology of delta ferrite is dependent. Weld Res Suppl 362s-374s

15. J.A. Brooks and A.W. Thompson (1991) Microstructural development and solidification cracking susceptibility of austenitic stainless steel welds. Int Mater Rev 36:16–44

16. Gill TPS, Mudali UK, Seetharaman V, Gnanamoorthy JB (1988) Effect of heat input and microstructure on pitting corrosion in AISI 316L submerged arc welds. Corrosion 44:511–516

17. Leinonen H (1995) Stress corrosion cracking and life prediction of austenitic stainless steels in calcium chloride solution. CORROSION 52:337–346

18. Puiggali M, Desjardins D, Ajana L (1987) A critical study of stress corrosion cracking testing methods for stainless steels in hot chloride media. Corros Sci 27:585–594. https://doi.org/10.1016/0010-938X(87)90032-1

19. Pugh EN (1971) The theory of stress corrosion cracking in alloys. by JC Scully 418

20. Mukai Y, Watanabe M (1978) M, Murata: Fractography in Failure Analysis, ASTM STP 645. ASTM, Philadelphia, PA 164–175

21. Muraleedharan P, Khatak HS, Gnanamoorthy JB, Rodriguez P (1985) Effect of cold work on stress corrosion cracking behavior of types 304 and 316 stainless steels. Metall Trans A 16:285–289